

Observation of collective charge excitations in a cuprate superconductor

Xunyang Hong,¹ Yujie Yan,² L. Martinelli,¹ I. Biało,¹ K. von Arx,¹ J. Choi,^{3,4} Y. Sassa,⁵ S. Pyon,⁶ T. Takayama,⁷ H. Takagi,^{7,8} Zhenglu Li,⁹ M. Garcia-Fernandez,³ Ke-Jin Zhou,³ J. Chang,^{1,*} and Qisi Wang^{2,†}

¹*Physik-Institut, Universität Zürich, Winterthurerstrasse 190, CH-8057 Zürich, Switzerland*

²*Department of Physics, The Chinese University of Hong Kong, Shatin, Hong Kong, China*

³*Diamond Light Source, Harwell Campus, Didcot, Oxfordshire OX11 0DE, United Kingdom*

⁴*Department of Physics, Korea Advanced Institute of Science and Technology,
291 Daehak-ro, Daejeon 34141, Republic of Korea*

⁵*Department of Applied Physics, KTH Royal Institute of Technology, SE-106 91 Stockholm, Sweden*

⁶*Department of Applied Physics, The University of Tokyo, Tokyo 113-8656, Japan*

⁷*Max Planck Institute for Solid State Research, 70569 Stuttgart, Germany*

⁸*Department of Physics, The University of Tokyo, Tokyo 113-0033, Japan*

⁹*Mork Family Department of Chemical Engineering and Materials Science,
University of Southern California, Los Angeles, CA, 90089, USA*

Emergent symmetry breakings in condensed matter systems are often intimately linked to collective excitations. For example, the intertwined spin-charge stripe order in cuprate superconductors is associated with spin and charge excitations. While the collective behavior of spin excitations is well established, the nature of charge excitations remains to be understood. Here we present a high-resolution resonant inelastic x-ray scattering (RIXS) study of charge excitations in the stripe-ordered cuprate $\text{La}_{1.675}\text{Eu}_{0.2}\text{Sr}_{0.125}\text{CuO}_4$. The RIXS spectra consist of both charge and phonon excitations around the charge ordering wave vector. By modeling the momentum-dependent phonon intensity, the charge-excitation spectral weight is extracted for a wide range of energy. As such, we reveal the highly dispersive nature of the charge excitations, with an energy scale comparable to the spin excitations. Since charge order and superconductivity in cuprates are possibly driven by the same electronic correlations, determining the interaction strength underlying charge order is essential to establishing a comprehensive microscopic model of high-temperature superconductivity.

Correlated electron systems often exhibit a variety of collective excitations that encode the nature of their ground state instabilities. For example, in cuprate superconductors, spin excitations with a large bandwidth (~ 300 meV) reveal the existence of strong magnetic correlations and large exchange couplings that span the entire doping phase diagram [1]. These observations have led to the idea that spin fluctuations are primarily responsible for the formation of Cooper pairs in these ma-

terials [2, 3]. Besides magnetic correlations, experiments have established the universal presence of charge correlations in hole-doped cuprates [4–8] with a possible link to superconductivity and the pseudogap phase [9–13]. While static charge order is found to compete with superconductivity [14], its bosonic excitations could potentially generate attractive interactions between electrons and promote superconductivity [12, 15]. Recent studies further suggest charge fluctuations to be responsible for the strange metal behavior [16] and the pseudogap formation [9, 11]. These findings have rendered charge dynamics a crucial factor for understanding the low-energy physics of the cuprates. In particular, determining the interaction strength behind charge order is crucial for establishing the effective model that describes the complex phase diagram of cuprates [17–20]. However, it has been a challenging experimental task to directly resolve collective charge excitations. How the charge excitations influence the electronic properties of the cuprates, therefore, remains an outstanding question.

With the improvement of the energy resolution, resonant inelastic x-ray scattering (RIXS) has been established as an effective probe of low-energy excitations [21]. The enhanced sensitivity to charge correlations is especially useful for studies of strongly correlated systems. Recent RIXS studies on several cuprate systems have revealed anomalies of phonon dispersions and intensities near the charge ordering wave vector [22–27], implying a possible charge excitation mode that intersects the phonon modes. Notably, a low-energy excitation mode with a characteristic energy scale of ~ 10 meV has been observed near the charge ordering wave vector [16, 24, 26, 28]. This low-energy mode, identified as charge density fluctuations, has been proposed to account for the strange metal behavior [16]. Yet, due to the interference between the weak charge excitations and

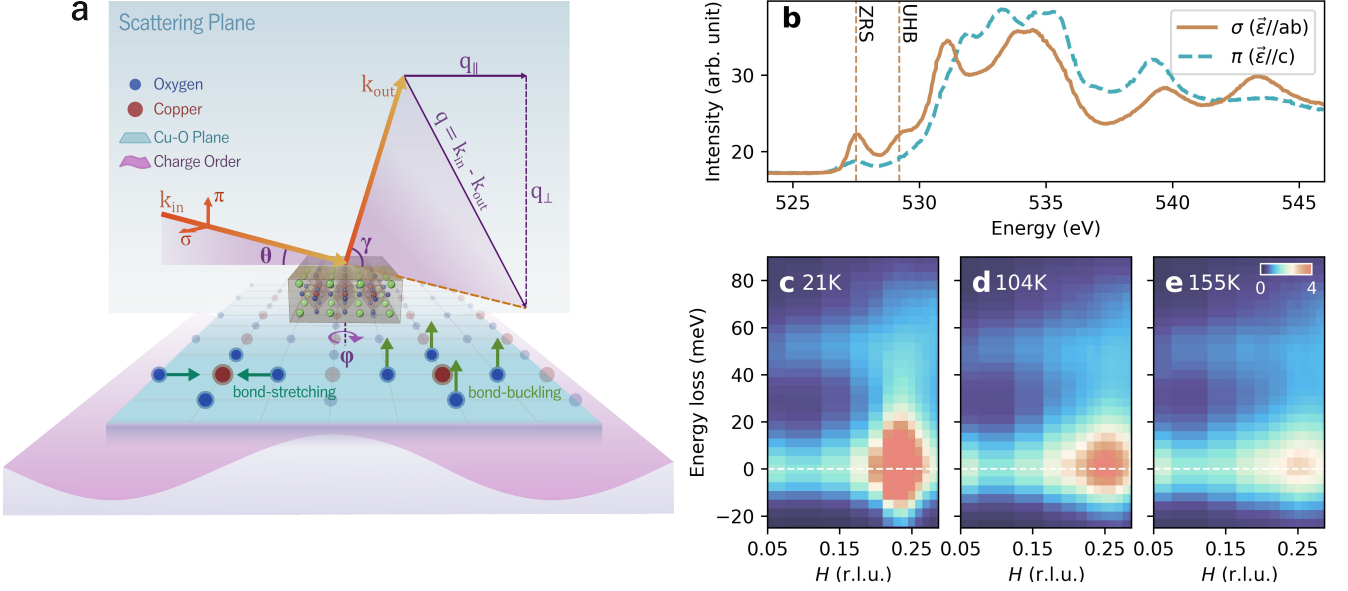


FIG. 1. **Crystal structure, phonon modes, XAS, and RIXS intensity map.** (a) Schematic of the RIXS experiment. Momentum transfer \mathbf{q} between the incident (\mathbf{k}_{in}) and scattered (\mathbf{k}_{out}) photons is projected into components within (\mathbf{q}_{\parallel}) and perpendicular to (\mathbf{q}_{\perp}) the Cu-O planes. Green arrows illustrate the bond-stretching (in-plane) and bond-buckling (out-of-plane) phonon modes. (b) XAS spectra (measured by total-electron-yield) collected with a grazing-incidence angle of $\theta = 20^\circ$ using σ and π light polarizations. (c-e) RIXS intensity map as a function of energy loss and momentum transfer at indicated temperature. White dashed lines represent the zero energy loss.

various phonon modes, it has been difficult to extract the charge excitation spectral weight. As such, essential information including the dispersion and energy scale of charge excitation mode remains unknown.

Here, we employ oxygen K -edge RIXS to investigate the low-energy excitations in $\text{La}_{1.8-x}\text{Eu}_{0.2}\text{Sr}_x\text{CuO}_4$ with $x = 0.125$ (Eu-LSCO), which exhibits a strong charge order [29]. By modeling the RIXS phonon cross sections, we extract the spectral weight of charge excitations as a function of momentum and energy transfers $S(\mathbf{q}, \omega)$. At low temperature ($T = 21$ K) the charge excitation mode emerges from the ordering wave vector and disperses outwards with a velocity of $v_c \sim 800$ meV \AA up to at least ~ 60 meV. Such an energy scale is comparable to the paramagnon bandwidth, implying the connection to the spin order as proposed within the framework of fluctuating stripes. The highly dispersive character reveals the collective nature of charge excitations, which may have profound impact on the superconducting and the normal state properties.

Results

X-ray absorption spectroscopy (XAS) measurements were performed across the oxygen K -edge resonance using σ and π polarizations with grazing-incidence geometry (Fig. 1b). The pre-edge at ~ 527.5 eV is commonly interpreted as a Zhang-Rice singlet (ZRS) state [30, 31], where an oxygen $1s$ electron is excited into the unoc-

cupied oxygen $2p$ ligand hole state ($3d^9\bar{L} \rightarrow 1s3d^9$). The peak at ~ 529 eV originates from the excitation of a $1s$ core electron to the upper Hubbard band (UHB, $3d^9 \rightarrow 1s3d^{10}$). Both the ZRS and UHB peaks are enhanced with σ light polarisation, indicating a dominant in-plane electronic nature.

RIXS measurements were performed at the ZRS peak energy (~ 527.5 eV) which has enhanced sensitivity to the doped holes. RIXS intensity maps as a function of in-plane momentum transfer $\mathbf{q} = (H, 0)$ and energy loss at three selected temperatures are shown in Fig. 1(c-e). Consistent with previous resonant and non-resonant x-ray scattering studies [8, 23, 24, 29, 32–36], the charge order reflection at $\mathbf{q}_{CO} = (q_{CO}, 0)$, with $q_{CO} \approx 0.23$, weakens with increasing temperature. The broad feature in momentum at 155 K indicates a dynamical and short-range nature of the charge correlations at high temperature [29]. These RIXS spectra display multiple excitation modes below ~ 100 meV. Exemplary spectra at $\mathbf{q} = (H, 0)$ with $H = 0.15$ and 0.23 are shown in Fig. 2(a,b). Inelastic signals near 50 meV and 70 meV have previously been attributed to bond-buckling and bond-stretching phonon modes, respectively [24, 37] (see Fig. 1a). Thus, the line shape is fitted using five components. The elastic scattering and two inelastic modes above 40 meV are described by Voigt functions – see grey, light green, and dark green components. To account for the asymmetric line shape around the elastic component, a low-energy mode – modeled by a Gaussian function

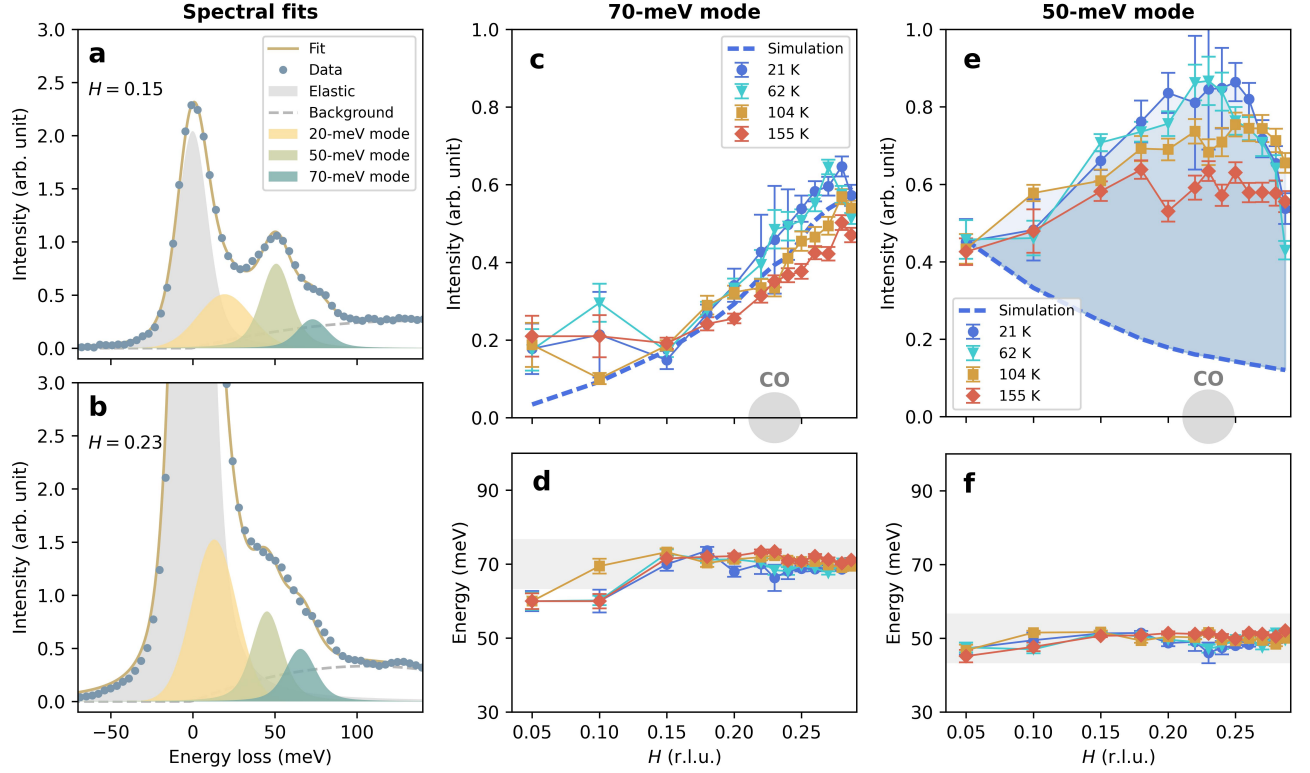


FIG. 2. **Low-energy excitations probed by RIXS.** (a,b) Representative RIXS spectra recorded away and near the charge ordering wave vector at base temperature (21 K). The brown solid line is a fit including elastic scattering (grey), a charge (yellow), and two phonon (light green and dark green) excitation modes on top of a background (grey dashed line). (c,d) The intensity as a function of momentum of the 70-meV mode and its dispersion. (e,f) The intensity and dispersion of the 50-meV mode. The blue shaded area indicates the additional intensity of the excitation in comparison to the phonon simulation. The dashed lines in (c,e) are obtained from phonon simulation (see text); Grey shaded area in (d,f) is a guide to the eye. CO, charge order.

(yellow profile) – is included. Finally, the background is modeled by a second-order polynomial function (grey dashed line). In the following text, we refer to the three inelastic modes as 20-meV, 50-meV, and 70-meV modes, respectively.

The dispersion relations of the 50- and 70-meV modes are shown in Figs. 2d and 2f, respectively. Both modes display weak or moderate dispersion with no clear softening effect around the charge ordering wave vector. The peak amplitudes of the 70- and 50-meV modes are shown in Figs. 2c and 2e as a function of momentum transfer. An enhancement of intensity is observed around the charge ordering wave vector for the 50-meV excitation, which decreases with increasing temperature. This behavior significantly deviates from the temperature evolution of a phonon mode. To further understand this observation, we calculate the momentum-dependent RIXS intensity of the bond-stretching and bond-buckling phonon modes, respectively, and plot the results as dashed lines (see Methods for a description of the phonon simulation). The calculation shows good agreement with the experimental data for the 70-meV mode, which corresponds

to the energy scale of the bond-stretching phonon mode. By contrast, the simulation substantially underestimates the excitation spectral weight around the charge ordering wave vector for the 50-meV excitation.

In Fig. 3, we summarize the temperature dependence. The elastic scattering intensity as a function of momentum transfer ($H, 0$) is shown in Fig. 3a for the temperatures indicated. Similarly, in Fig. 3b we plot the amplitude of the 20-meV excitation as a function of momentum transfer for the same temperatures. We stress that the elastic and the inelastic components display distinct temperature dependencies. As mentioned before, the simulated bond-buckling phonon intensity does not fully account for the observed spectral weight of the 50-meV mode. To understand this observation, we extract the additional excitation intensity by subtracting the simulation from the observed amplitude – see Fig. 3c. In the following paragraphs, we refer to this as the *subtracted* amplitude of the 50-meV mode.

The elastic and inelastic components are integrated around the peak centre over a momentum window as indicated by the shaded area in Fig. 3(a-c). The result-

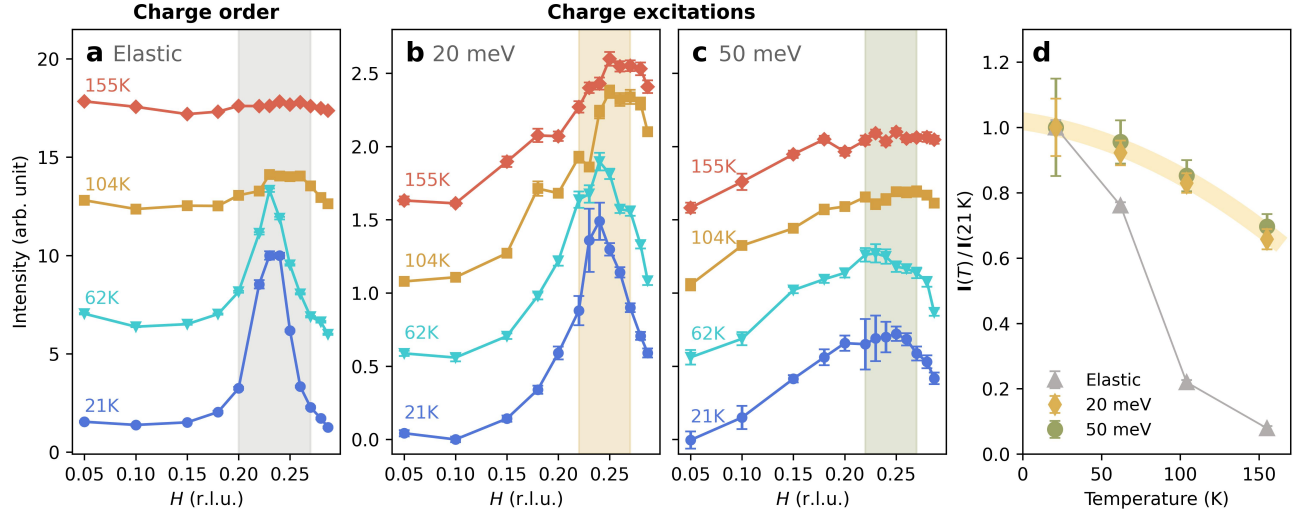


FIG. 3. **Temperature dependence of charge order and its fluctuations.** (a) Elastic scattering intensity (peak amplitude) along $(H, 0)$ versus temperatures as indicated. (b) Inelastic intensity of the 20-meV mode; (c) The amplitude of the subtracted 50-meV mode for the same temperatures as in (a,b). All data in (a-c) have been given an arbitrary shift to enhance visibility. Shaded area represents the integration window. (d) Integrated intensities of elastic and inelastic signals in (a-c) as functions of temperature. For comparison, the intensities are normalized to the value at the base temperature (21 K). The orange curve is a guide to the eye.

ing integrated intensities as a function of temperature are shown in Fig. 3d. The elastic signal decreases more rapidly with increasing temperature compared to the 20-meV excitation. We also stress that the subtracted 50-meV mode displays a temperature dependence similar to that of the 20-meV mode. This could suggest a common origin for these two components. Note that the intensity of the 70-meV excitation also exhibits a slight increase upon cooling at $H \gtrsim q_{CO}$, which may be further enhanced at a larger momentum transfer, as indicated by a previous Cu L -edge RIXS study [38].

An alternative approach to analyze the data is to subtract the elastic line profile and the background signal. In Fig. 4a, we present the RIXS intensity map at 21 K, with the elastic scattering and background subtracted. Fig. 4b further displays the momentum-dependent signal for the indicated excitation energy (orange data points). For comparison, the amplitudes of the 20-meV mode (black circles) and the subtracted 50-meV mode (red diamonds) are also plotted in the same figure, demonstrating consistent results from both analysis approaches. The signal weakens and broadens in momentum as the energy increases. At higher energies ($\gtrsim 40$ meV), a two-peak feature can be discerned. Therefore, we applied a double-Gaussian fit model to capture the broadening effect, as illustrated by the orange shaded area in Fig. 4b.

Discussion

Our key observation is the existence of low-energy excitations that exhibit a temperature dependence distinct from the charge order, and also different from what is

expected from phonons. A prevalent interpretation is that these low-energy excitations are the manifestation of charge fluctuations. In fact, phonon anomalies near the charge ordering wave vectors have been interpreted as evidence of charge fluctuations [22, 25, 39]. Furthermore, their quantum critical nature in cuprate has previously been discussed [16, 24]. In this work, we focused on the excitations well within the ordered state. An outstanding question is the propagating nature of these charge fluctuations. Extracting the dispersion of charge fluctuations has proven challenging due to the overlap with elastic signal and phonon contributions. A direct observation of dispersive charge excitations has thus far not been realized, hindering the understanding of the microscopic charge ordering mechanism.

The high energy resolution of RIXS enabled us to filter out the elastic scattering from, for example, charge fluctuations. By modeling the phonon modes with strong electron-phonon coupling, it is also possible to separate the spectral weight contributions from phonons and charge fluctuations. This step in our analysis relies on the calculation of momentum-dependent cross-section for the phonon modes, a method that has not been employed in this context before.

By eliminating the elastic scattering and the phonon contributions from the RIXS spectra, we are able to isolate the signal stemming from charge fluctuations. This remaining signal displays a significant dispersion. For simplicity, we assume the following dispersion relation: $\omega_{cf} = \sqrt{\Delta^2 + v_c^2 |\mathbf{q} - \mathbf{q}_{CO}|^2}$. Here, Δ denotes the energy gap, v_c is the excitation velocity (stiffness) around

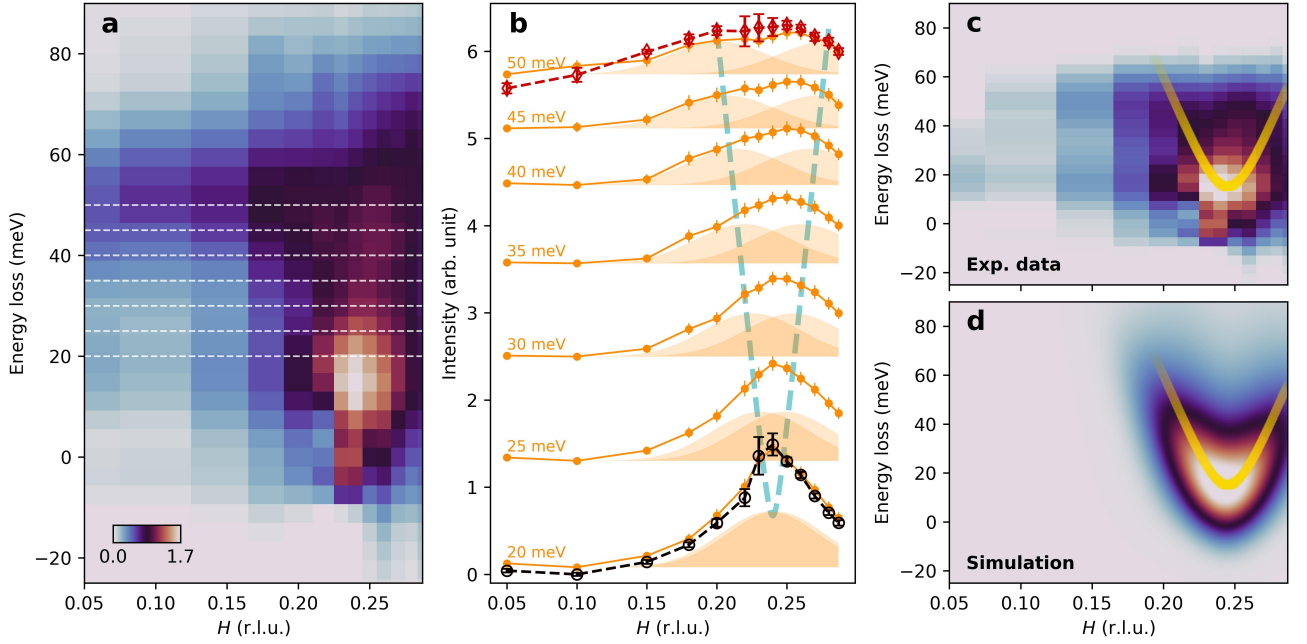


FIG. 4. **Dispersive charge order fluctuations.** (a) RIXS intensity map, with elastic and background signal subtracted, as a function of energy loss and momentum transfer at 21 K. Horizontal white dashed lines represent the energy cut we made for the data shown in (b). (b) Momentum dependence of RIXS intensities, with elastic and background signal subtracted, at constant energy loss as indicated. The energy integration window is 5 meV. For comparison, intensities shown in Fig. 3 are overlaid: Black circles are amplitude of the 20-meV mode, while red diamonds are the phonon-signal-subtracted amplitude of the 50-meV mode. Shaded area represents the fitted double-Gaussian model. Blue dashed line depicts the shift of the two Gaussian functions as energy increases. (c) RIXS intensity map, with elastic, background signal, and phonon simulated signal subtracted. Yellow curve is the modeled dispersion of the charge fluctuation. (d) Simulation of charge order fluctuation $S(\mathbf{q}, \omega)$ using the parameters obtained from the fits in (b).

the charge ordering wave vector $\mathbf{q}_{\text{CO}} \approx (0.23, 0)$. Our data suggest a charge fluctuation velocity (stiffness) of $v_c = (800 \pm 200) \text{ meV } \text{\AA}$, which is comparable to that of the paramagnons ($v_s \sim 800 \text{ meV } \text{\AA}$ [40]). The comparable energy scales likely originate from the intimate coupling between the spin and charge orders.

Previous RIXS studies have estimated the charge excitation velocity based on indirect observations, e.g., anomalies in the phonon intensity away from \mathbf{q}_{CO} [22, 25, 39], or by modeling the charge excitation intensity below the bond-buckling phonon energy [24]. The velocity values derived from these estimations exhibit large discrepancies, ranging from 450 to 1300 $\text{meV } \text{\AA}$. This large uncertainty has hindered our fundamental understanding of the related quasi-particle and its impact on the normal state and superconducting properties. Here, by modeling carefully the RIXS phonon responses, we isolate the charge excitation contributions and directly establish a dispersive charge excitation mode extending to at least 60 meV (Fig. 4c). Similar attempts but with different strategies have been made, for example, by subtracting the scattering intensity along the diagonal (H, H) direction [16], or by assuming the momentum-dependent phonon contribution as a simple polynomial

background [12]. Although these works revealed the existence of charge fluctuations, the dispersion has never been determined.

In contrast to cuprate systems with weaker charge orders or closer to the quantum critical point (QCP), where charge excitations appear as a continuum [16, 24, 39], charge order in Eu-LSCO $x = 0.125$ manifests as a renormalized classical order. As such, the charge excitations observed in this compound directly reflect the interaction strength governing charge ordering. This is analogous to the distinction between spin waves in a magnetically ordered state and the damped excitations near a magnetic QCP [41–43]. Therefore, the collective excitations observed here provide a clearer insight into the nature of the underlying charge dynamics rather than the effects dominated by quantum fluctuations [16, 24, 39].

The quantitative determination of charge excitation dispersion is crucial for establishing the underlying interactions that involve both the spin and charge degrees of freedom. The comparable energy scales of collective charge and spin excitations suggest a strong coupling realized in the form of fluctuating stripes [44]. As pairing does not coexist with local antiferromagnetic order, charge fluctuations may enhance Josephson coupling be-

tween neighbouring stripes and promote superconductivity [13]. In this context, collective charge excitations may contribute constructively to superconductivity. In fact, numerical calculations have shown that electron-electron (exchange) interactions that mediate pairing could also be responsible for charge ordering [17, 19, 20]. This theoretical insight aligns with our observation of a common energy scale for charge and spin excitations, as well as the superconducting gap. Besides superconductivity, charge fluctuations may also profoundly influence the normal state properties. It has recently been suggested that electron dissipation due to scattering from charge fluctuations leads to the strange metal behavior [16]. Such a scenario can be further verified by establishing the evolution of the charge excitation dispersion and normal state electronic properties throughout the phase diagram.

By integrating phonon cross-section calculation and high-resolution RIXS experiments, our study successfully isolated weak charge excitations and established their dispersion and energy scale in cuprates. This approach can be extended to other strongly correlated materials, including nickelate and iron-based superconductors, where charge-spin coupling is significant [45–49]. As such, our study lays the groundwork for uncovering universal behaviors that link charge dynamics to emergent phases in complex quantum materials.

Methods

RIXS experiments

High-quality Eu-LSCO single crystals were grown using the floating zone method and studied at the I21 beamline of Diamond Light Source [50]. RIXS experiments were carried out at the O K -edge resonance (~ 527.5 eV). Grazing-incidence geometry with linear vertical (σ) incident light polarization was employed to enhance the cross sections of charge and phonon excitations. The energy resolution, determined from the elastic scattering of amorphous carbon, was measured to have a full width at half maximum (FWHM) of 22.5 meV. The wave vector \mathbf{q} at (q_x, q_y, q_z) was defined as $(H, K, L) = (q_x a/2\pi, q_y b/2\pi, q_z c/2\pi)$ in reciprocal lattice units (r.l.u.) using pseudo-tetragonal notation, with $a \approx b \approx 3.79$ Å and $c \approx 13.1$ Å. The scattering angle was fixed at $\gamma = 154^\circ$. The magnitude and direction of the in-plane momentum transfer $\mathbf{q}_{\parallel} = (H, H \tan \phi)$ are controlled by the x-ray incident angle θ and sample azimuthal angle ϕ , respectively (Fig. 1a). To avoid the overwhelming elastic scattering at the charge ordering wave vector, the data were taken with $\phi = 4^\circ$ [38]. RIXS intensities were normalized to the weight of the dd excitations between 1.0 eV and 3.3 eV, as in refs. 4, 16, 23, and 38.

Phonon simulation

The RIXS intensities of the bond-buckling and bond-

stretching phonon modes are calculated by a diagrammatic method [51]:

$$I_\nu(\mathbf{q}, \Omega) = \sum_{\mathbf{k}, \mathbf{k}'} G[g] P[\phi] E[\varepsilon_{\mathbf{k}}, D_\nu], \quad (1)$$

where I_ν is the RIXS intensity; \mathbf{q} and Ω are the momentum transfer and the energy loss, respectively; the subscript ν indicates the phonon mode; and \mathbf{k} is the momentum variable on the electron energy band $\varepsilon_{\mathbf{k}}$. In the equation, $G[g]$ is a function of electron-phonon coupling $g(\mathbf{k}, \mathbf{q})$, $P[\phi]$ is a function of orbital projecting function $\phi_{2p_x}(\mathbf{k})$, $E[\varepsilon_{\mathbf{k}}, D_\nu]$ is a function of energy band $\varepsilon_{\mathbf{k}}$ and phonon propagator $D_\nu(\mathbf{q})$ (see Supplementary Information for detailed descriptions).

The electron-phonon coupling $g(\mathbf{k}, \mathbf{q})$ is derived within a five-band model, see ref. 52. Specifically for the bond stretching and bond buckling modes, we have

$$\begin{aligned} g_{bs}(\mathbf{k}, \mathbf{q}) &= g_{bs}^0 \sqrt{\sin^2(q_x a/2) + \sin^2(q_y a/2)}, \\ g_{bb}(\mathbf{k}, \mathbf{q}) &= g_{bb}^0 [\sin(k_x a/2) \sin(p_x a/2) \cos(q_y a/2) \\ &\quad + \sin(k_y a/2) \sin(p_y a/2) \cos(q_x a/2)], \end{aligned} \quad (2)$$

where $\mathbf{p} \equiv \mathbf{k} - \mathbf{q}$. According to the discussion in ref. 52, the prefactor g_{bs}^0 and g_{bb}^0 are of the same order of magnitude. In our simulation, we adopted a ratio $g_{bb}^0/g_{bs}^0 = 0.9$ to obtain the best agreement with the experimental results.

The orbital projecting function $\phi_{2p_x}(\mathbf{k})$ can be calculated by projecting the oxygen $2p_x$ orbital onto the effective band. To obtain this projecting function, the effective three-orbital Hamiltonian consists of copper $3d_{x^2-y^2}$, oxygen $2p_x$ and $2p_y$ orbitals [53–55].

$$H = \sum_{\mathbf{k}, \sigma} \Psi_{\mathbf{k}, \sigma}^\dagger \begin{pmatrix} \epsilon_d & 2t_{pd}s_x & -2t_{pd}s_y \\ 2t_{pd}s_x & \tilde{\epsilon}_x(\mathbf{k}) & 4\tilde{t}_{pp}s_x s_y \\ -t_{pd}s_y & 4\tilde{t}_{pp}s_x s_y & \tilde{\epsilon}_y(\mathbf{k}) \end{pmatrix} \Psi_{\mathbf{k}, \sigma}, \quad (3)$$

$$\Psi_{\mathbf{k}, \sigma}^\dagger = \left(d_{\mathbf{k}, \sigma}^\dagger, p_{x, \mathbf{k}, \sigma}^\dagger, p_{y, \mathbf{k}, \sigma}^\dagger \right),$$

where $s_{x,y} = \sin(k_{x,y} a/2)$, $\tilde{\epsilon}_{x,y} = \epsilon_p + 4t_{pp}^i s_{x,y}^2$, $\Psi_{\mathbf{k}, \sigma}^\dagger$ is a vector of creation operators on $3d_{x^2-y^2}$, $2p_x$, and $2p_y$ orbitals, respectively. We adopted the parameters given in ref. 55: energy difference between copper $3d_{x^2-y^2}$ and oxygen $2p_{x,y}$ orbitals $\epsilon_d - \epsilon_p = 0.9$ eV; Hopping parameters $t_{pd} = 1.6$ eV, $\tilde{t}_{pp} = t_{pp}^i = -1$ eV. By diagonalizing the Hamiltonian, the projecting function ϕ_{2p_x} is the projection of the second basis vector onto the eigenvector with the highest eigenvalue.

The effective electronic structure $\varepsilon_{\mathbf{k}}$ is modeled using a single-band tight binding model:

$$\begin{aligned} \varepsilon_{\mathbf{k}} + \mu &= -2t_1 [\cos(k_x a) + \cos(k_y a)] \\ &\quad - 4t_2 \cos(k_x a) \cos(k_y a) \\ &\quad - 2t_3 [\cos(2k_x a) + \cos(2k_y a)]. \end{aligned} \quad (4)$$

Previous angle-resolved photoemission spectroscopy (ARPES) work suggests that tight binding parameters are very similar for LSCO and Eu-LSCO [56]. Thus, we use recently extracted values ($\mu/t = 0.7$, $t_2/t_1 = -0.15$, $t_3/t_2 = -0.5$ and $t = 190$ meV) from LSCO with doping $x \sim 1/8$ [57].

To model the charge fluctuation, an ansatz is made to capture its bosonic feature:

$$\chi(\mathbf{q}, \omega) = \frac{1}{\omega_{\text{cf}}^2 - (\omega + i\Gamma)^2}, \quad (5)$$

where χ is the susceptibility of the charge fluctuation, and Γ is the dissipation parameter. The dispersion is given by $\omega_{\text{cf}} = \sqrt{\Delta^2 + v_c^2 |\mathbf{q} - \mathbf{q}_{\text{CO}}|^2}$. The energy gap $\Delta = 18$ meV is estimated from the spectral fit shown in Fig. 2b. The dynamical structure factor can be expressed as

$$S(\mathbf{q}, \omega) = \left(1 - e^{-\frac{\hbar\omega}{k_B T}}\right)^{-1} \text{Im}\chi(\mathbf{q}, \omega), \quad (6)$$

where k_B is the Boltzmann constant.

Data availability

Data supporting the findings of this study are available from the corresponding authors upon reasonable request.

Acknowledgments

We thank Zheng-Cheng Gu, Di-Jing Huang, Hsiao-Yu Huang, and Yao Wang for insightful discussions. X.H., K.v.A. and J.Chang thank the Swiss National Science Foundation under Projects No. 200021_188564. Y.Y. and Q.W. are supported by the Research Grants Council of Hong Kong (ECS No. 24306223), and the CUHK Direct Grant (4053613 and 4053671). I.B. and L.M. acknowledge support from the Swiss Government Excellence Scholarship under project numbers ESKAS-Nr: 2022.0001 and ESKAS-Nr: 2023.0052. J.Choi acknowledges financial support from the National Research Foundation of Korea (NRF) funded by the Korean government (MSIT) through Sejong Science Fellowship (Grant No. RS-2023-00252768). Y.S. is supported by the Wallenberg Academy Fellows through the grant 2021-0150. We acknowledge Diamond Light Source for providing beam time on beamline I21 under Proposal MM29011.

Author contributions

J.Chang and Q.W. conceived the project. S.P., T.T. and H.T. grew the Eu-LSCO single crystals. RIXS experiments were performed by K.v.A., J. Choi, Y.S., M.G.F., K.J.Z., J.Chang and Q.W. Data analysis and phonon simulations were carried out by X.H. with assistance from Y.Y., L.M., I.B. and Z.L.. The manuscript was written by X.H., J.Chang and Q.W. with input from all

authors.

Competing interests

The authors declare no competing interests.

* johan.chang@physik.uzh.ch

† qwang@cuhk.edu.hk

- [1] M. P. M. Dean, G. Dellea, R. S. Springell, F. Yakhov-Harris, K. Kummer, N. B. Brookes, X. Liu, Y.-J. Sun, J. Strle, T. Schmitt, L. Braicovich, G. Ghiringhelli, I. Božović, and J. P. Hill, *Nat. Mater.* **12**, 1019 (2013).
- [2] D. J. Scalapino, *Rev. Mod. Phys.* **84**, 1383 (2012).
- [3] P. Monthoux, D. Pines, and G. G. Lonzarich, *Nature* **450**, 1177 (2007).
- [4] G. Ghiringhelli, M. L. Tacon, M. Minola, S. Blanco-Canosa, C. Mazzoli, N. B. Brookes, G. M. D. Luca, A. Frano, D. G. Hawthorn, F. He, T. Loew, M. M. Sala, D. C. Peets, M. Salluzzo, E. Schierle, R. Sutarto, G. A. Sawatzky, E. Weschke, B. Keimer, and L. Braicovich, *Science* **337**, 821 (2012).
- [5] Y. Y. Peng, M. Salluzzo, X. Sun, A. Ponti, D. Betto, A. M. Ferretti, F. Fumagalli, K. Kummer, M. Le Tacon, X. J. Zhou, N. B. Brookes, L. Braicovich, and G. Ghiringhelli, *Phys. Rev. B* **94**, 184511 (2016).
- [6] E. H. da Silva Neto, P. Aynajian, A. Frano, R. Comin, E. Schierle, E. Weschke, A. Gyenis, J. Wen, J. Schneeloch, Z. Xu, S. Ono, G. Gu, M. Le Tacon, and A. Yazdani, *Science* **343**, 393 (2014).
- [7] L. Chaix, B. Lebert, H. Miao, A. Nicolaou, F. Yakhov, H. Cercellier, S. Grenier, N. B. Brookes, A. Sulpice, S. Tsutsui, A. Bosak, L. Paolasini, D. Santos-Cottin, H. Yamamoto, I. Yamada, M. Azuma, T. Nishikubo, T. Yamamoto, M. Katsumata, M. P. M. Dean, and M. d'Astuto, *Phys. Rev. Research* **4**, 033004 (2022).
- [8] W. Tabis, B. Yu, I. Bialo, M. Bluschke, T. Kolodziej, A. Kozłowski, E. Blackburn, K. Sen, E. M. Forgan, M. v. Zimmermann, Y. Tang, E. Weschke, B. Vignolle, M. Hep-ting, H. Gretarsson, R. Sutarto, F. He, M. Le Tacon, N. Barišić, G. Yu, and M. Greven, *Phys. Rev. B* **96**, 134510 (2017).
- [9] S. Caprara, C. Di Castro, G. Seibold, and M. Grilli, *Phys. Rev. B* **95**, 224511 (2017).
- [10] A. Perali, C. Castellani, C. D. Castro, and M. Grilli, *Phys. Rev. B* **54**, 16216 (1996).
- [11] Z.-Y. Yue, Z.-T. Xu, S. Yang, and Z.-C. Gu, *arXiv:2404.16770* (2024).
- [12] B. Yu, W. Tabis, I. Bialo, F. Yakhov, N. B. Brookes, Z. Anderson, Y. Tang, G. Yu, and M. Greven, *Phys. Rev. X* **10**, 021059 (2020).
- [13] S. A. Kivelson, E. Fradkin, and V. J. Emery, *Nature* **393**, 550 (1998).
- [14] J. Chang, C. Niedermayer, R. Gilardi, N. B. Christensen, H. M. Rønnow, D. F. McMorrow, M. Ay, J. Stahn, O. Sobolev, A. Hiess, S. Pailhes, C. Baines, N. Momono, M. Oda, M. Ido, and J. Mesot, *Phys. Rev. B* **78**, 104525 (2008).
- [15] Y. Wang and A. V. Chubukov, *Phys. Rev. B* **92**, 125108 (2015).

- [16] R. Arpaia, L. Martinelli, M. M. Sala, S. Caprara, A. Nag, N. B. Brookes, P. Camisa, Q. Li, Q. Gao, X. Zhou, M. Garcia-Fernandez, K.-J. Zhou, E. Schierle, T. Bauch, Y. Y. Peng, C. Di Castro, M. Grilli, F. Lombardi, L. Braicovich, and G. Ghiringhelli, *Nat. Commun.* **14**, 7198 (2023).
- [17] J. C. S. Davis and D.-H. Lee, *Proc. Natl. Acad. Sci. U.S.A.* **110**, 17623 (2013).
- [18] S. Sachdev and R. La Placa, *Phys. Rev. Lett.* **111**, 027202 (2013).
- [19] B.-X. Zheng, C.-M. Chung, P. Corboz, G. Ehlers, M.-P. Qin, R. M. Noack, H. Shi, S. R. White, S. Zhang, and G. K.-L. Chan, *Science* **358**, 1155 (2017).
- [20] E. W. Huang, C. B. Mendl, S. Liu, S. Johnston, H.-C. Jiang, B. Moritz, and T. P. Devereaux, *Science* **358**, 1161 (2017).
- [21] L. J. P. Ament, M. van Veenendaal, T. P. Devereaux, J. P. Hill, and J. van den Brink, *Rev. Mod. Phys.* **83**, 705 (2011).
- [22] J. Li, A. Nag, J. Pelliciari, H. Robarts, A. Walters, M. Garcia-Fernandez, H. Eisaki, D. Song, H. Ding, S. Johnston, R. Comin, and K.-J. Zhou, *Proc. Natl. Acad. Sci. U.S.A.* **117**, 16219 (2020).
- [23] J. Q. Lin, H. Miao, D. G. Mazzone, G. D. Gu, A. Nag, A. C. Walters, M. Garcia-Fernandez, A. Barbour, J. Pelliciari, I. Jarrige, M. Oda, K. Kurosawa, N. Momono, K.-J. Zhou, V. Bisogni, X. Liu, and M. P. M. Dean, *Phys. Rev. Lett.* **124**, 207005 (2020).
- [24] H. Y. Huang, A. Singh, C. Y. Mou, S. Johnston, A. F. Kemper, J. van den Brink, P. J. Chen, T. K. Lee, J. Okamoto, Y. Y. Chu, J. H. Li, S. Komiya, A. C. Komarek, A. Fujimori, C. T. Chen, and D. J. Huang, *Phys. Rev. X* **11**, 041038 (2021).
- [25] L. Chaix, G. Ghiringhelli, Y. Y. Peng, M. Hashimoto, B. Moritz, K. Kummer, N. B. Brookes, Y. He, S. Chen, S. Ishida, Y. Yoshida, H. Eisaki, M. Salluzzo, L. Braicovich, Z.-X. Shen, T. P. Devereaux, and W.-S. Lee, *Nat. Phys.* **13**, 952 (2017).
- [26] Q. Li, H.-Y. Huang, T. Ren, E. Weschke, L. Ju, C. Zou, S. Zhang, Q. Qiu, J. Liu, S. Ding, A. Singh, O. Prokhnenko, D.-J. Huang, I. Esterlis, Y. Wang, Y. Xie, and Y. Peng, *Phys. Rev. Lett.* **131**, 116002 (2023).
- [27] Y. Y. Peng, A. A. Husain, M. Mitrano, S. X.-L. Sun, T. A. Johnson, A. V. Zakrzewski, G. J. MacDougall, A. Barbour, I. Jarrige, V. Bisogni, and P. Abbamonte, *Phys. Rev. Lett.* **125**, 097002 (2020).
- [28] L. Martinelli, I. Bialo, X. Hong, J. Oppliger, C. Lin, T. Schaller, J. Küspert, M. H. Fischer, T. Kurosawa, N. Momono, M. Oda, J. Choi, S. Agrestini, M. Garcia-Fernandez, K.-J. Zhou, Q. Wang, and J. Chang, *arXiv:2406.15062* (2024).
- [29] Q. Wang, M. Horio, K. von Arx, Y. Shen, D. John Mukkattukavil, Y. Sassa, O. Ivashko, C. E. Matt, S. Pyon, T. Takayama, H. Takagi, T. Kurosawa, N. Momono, M. Oda, T. Adachi, S. M. Haidar, Y. Koike, Y. Tseng, W. Zhang, J. Zhao, K. Kummer, M. Garcia-Fernandez, K.-J. Zhou, N. B. Christensen, H. M. Rønnow, T. Schmitt, and J. Chang, *Phys. Rev. Lett.* **124**, 187002 (2020).
- [30] C. T. Chen, F. Sette, Y. Ma, M. S. Hybertsen, E. B. Stechel, W. M. C. Foulkes, M. Schultze, S.-W. Cheong, A. S. Cooper, L. W. Rupp, B. Batlogg, Y. L. Soo, Z. H. Ming, A. Krol, and Y. H. Kao, *Phys. Rev. Lett.* **66**, 104 (1991).
- [31] S. Lee, E. W. Huang, T. A. Johnson, X. Guo, A. A. Husain, M. Mitrano, K. Lu, A. V. Zakrzewski, G. A. de la Peña, Y. Peng, H. Huang, S.-J. Lee, H. Jang, J.-S. Lee, Y. I. Joe, W. B. Doriese, P. Szypryt, D. S. Swetz, S. Chi, A. A. Aczel, G. J. MacDougall, S. A. Kivelson, E. Fradkin, and P. Abbamonte, *Proc. Natl. Acad. Sci. U.S.A.* **119**, e2119429119 (2022).
- [32] Q. Wang, K. von Arx, D. G. Mazzone, S. Mustafi, M. Horio, J. Küspert, J. Choi, D. Bucher, H. Wo, J. Zhao, W. Zhang, T. C. Asmara, Y. Sassa, M. Månsson, N. B. Christensen, M. Janoschek, T. Kurosawa, N. Momono, M. Oda, M. H. Fischer, T. Schmitt, and J. Chang, *Nat. Commun.* **13**, 1795 (2022).
- [33] H. Miao, J. Lorenzana, G. Seibold, Y. Y. Peng, A. Amorese, F. Yakhov-Harris, K. Kummer, N. B. Brookes, R. M. Konik, V. Thampy, G. D. Gu, G. Ghiringhelli, L. Braicovich, and M. P. M. Dean, *Proc. Natl. Acad. Sci. U.S.A.* **114**, 12430 (2017).
- [34] H. Miao, R. Fumagalli, M. Rossi, J. Lorenzana, G. Seibold, F. Yakhov-Harris, K. Kummer, N. B. Brookes, G. D. Gu, L. Braicovich, G. Ghiringhelli, and M. P. M. Dean, *Phys. Rev. X* **9**, 031042 (2019).
- [35] J. Choi, Q. Wang, S. Jöhr, N. Christensen, J. Küspert, D. Bucher, D. Biscette, M. Fischer, M. Hücker, T. Kurosawa, N. Momono, M. Oda, O. Ivashko, M. Zimmermann, M. Janoschek, and J. Chang, *Phys. Rev. Lett.* **128**, 207002 (2022).
- [36] N. B. Christensen, J. Chang, J. Larsen, M. Fujita, M. Oda, M. Ido, N. Momono, E. M. Forgan, A. T. Holmes, J. Mesot, M. Hücker, and M. v. Zimmermann, *arXiv:1404.3192* (2014).
- [37] F. Giustino, M. L. Cohen, and S. G. Louie, *Nature* **452**, 975 (2008).
- [38] Q. Wang, K. von Arx, M. Horio, D. J. Mukkattukavil, J. Küspert, Y. Sassa, T. Schmitt, A. Nag, S. Pyon, T. Takayama, H. Takagi, M. Garcia-Fernandez, K.-J. Zhou, and J. Chang, *Sci. Adv.* **7**, eabg7394 (2021).
- [39] W. S. Lee, K.-J. Zhou, M. Hepting, J. Li, A. Nag, A. C. Walters, M. Garcia-Fernandez, H. C. Roberts, M. Hashimoto, H. Lu, B. Nosarzewski, D. Song, H. Eisaki, Z. X. Shen, B. Moritz, J. Zaanen, and T. P. Devereaux, *Nat. Phys.* **17**, 53 (2020).
- [40] R. Coldea, S. M. Hayden, G. Aeppli, T. G. Perring, C. D. Frost, T. E. Mason, S.-W. Cheong, and Z. Fisk, *Phys. Rev. Lett.* **86**, 5377 (2001).
- [41] H. v. Löhneysen, A. Rosch, M. Vojta, and P. Wölfle, *Rev. Mod. Phys.* **79**, 1015 (2007).
- [42] C. Lester, S. Ramos, R. S. Perry, T. P. Croft, M. Laver, R. I. Bewley, T. Guidi, A. Hiess, A. Wildes, E. M. Forgan, and S. M. Hayden, *Nat. Commun.* **12**, 5798 (2021).
- [43] G. Aeppli, T. E. Mason, S. M. Hayden, H. A. Mook, and J. Kulda, *Science* **278**, 1432 (1997).
- [44] S. A. Kivelson, I. P. Bindloss, E. Fradkin, V. Oganessian, J. M. Tranquada, A. Kapitulnik, and C. Howald, *Rev. Mod. Phys.* **75**, 1201 (2003).
- [45] W. Li, Y. Zhang, P. Deng, Z. Xu, S.-K. Mo, M. Yi, H. Ding, M. Hashimoto, R. G. Moore, D.-H. Lu, X. Chen, Z.-X. Shen, and Q.-K. Xue, *Nat. Phys.* **13**, 957 (2017).
- [46] Z. Chen, D. Li, Z. Lu, Y. Liu, J. Zhang, Y. Li, R. Yin, M. Li, T. Zhang, X. Dong, Y.-J. Yan, and D.-L. Feng, *Nat. Commun.* **14**, 2023 (2023).
- [47] K. Bu, W. Zhang, Y. Fei, Y. Zheng, F. Ai, Z. Wu, Q. Wang, H. Wo, J. Zhao, and Y. Yin, *Nat. Commun.* (2024).

- [12](#), 1385 (2021).
- [48] H. Sun, M. Huo, X. Hu, J. Li, Z. Liu, Y. Han, L. Tang, Z. Mao, P. Yang, B. Wang, J. Cheng, D.-X. Yao, G.-M. Zhang, and M. Wang, [Nature](#) **621**, 493 (2023).
 - [49] J. Zhang, D. Phelan, A. S. Botana, Y.-S. Chen, H. Zheng, M. Krogstad, S. G. Wang, Y. Qiu, J. A. Rodriguez-Rivera, R. Osborn, S. Rosenkranz, M. R. Norman, and J. F. Mitchell, [Nat. Commun.](#) **11**, 6003 (2020).
 - [50] K.-J. Zhou, A. Walters, M. Garcia-Fernandez, T. Rice, M. Hand, A. Nag, J. Li, S. Agrestini, P. Garland, H. Wang, S. Alcock, I. Nistea, B. Nutter, N. Rubies, G. Knap, M. Gaughran, F. Yuan, P. Chang, J. Emmins, and G. Howell, [J. Synchrotron Radiat.](#) **29**, 563 (2022).
 - [51] T. P. Devereaux, A. M. Shvaika, K. Wu, K. Wohlfeld, C. J. Jia, Y. Wang, B. Moritz, L. Chaix, W.-S. Lee, Z.-X. Shen, G. Ghiringhelli, and L. Braicovich, [Phys. Rev. X](#) **6**, 041019 (2016).
 - [52] S. Johnston, F. Vernay, B. Moritz, Z.-X. Shen, N. Nagaosa, J. Zaanen, and T. P. Devereaux, [Phys. Rev. B](#) **82**, 064513 (2010).
 - [53] O. Andersen, A. Liechtenstein, O. Jepsen, and F. Paulsen, [J. Phys. Chem. Solids](#) **56**, 1573 (1995).
 - [54] W. A. Atkinson, A. P. Kampf, and S. Bulut, [New J. Phys.](#) **17**, 013025 (2015).
 - [55] S. Banerjee, W. A. Atkinson, and A. P. Kampf, [Commun. Phys.](#) **3**, 161 (2020).
 - [56] M. Horio, K. Hauser, Y. Sassa, Z. Mingazheva, D. Sutter, K. Kramer, A. Cook, E. Nocerino, O. Forslund, O. Tjernberg, M. Kobayashi, A. Chikina, N. Schröter, J. Krieger, T. Schmitt, V. Strocov, S. Pyon, T. Takayama, H. Takagi, O. Lipscombe, S. Hayden, M. Ishikado, H. Eisaki, T. Neupert, M. Månsson, C. Matt, and J. Chang, [Phys. Rev. Lett.](#) **121**, 077004 (2018).
 - [57] Y. Zhong, Z. Chen, S.-D. Chen, K.-J. Xu, M. Hashimoto, Y. He, S.-i. Uchida, D. Lu, S.-K. Mo, and Z.-X. Shen, [Proc. Natl. Acad. Sci. U.S.A.](#) **119**, e2204630119 (2022).